Palm vein recognition based on competitive coding scheme using multi-scale local binary pattern with ant colony optimization

Yassir Aberni, Larbi Boubchir, Boubaker Daachi

Pattern Recognition Letters
journal homepage: www.elsevier.com

Palm Vein Recognition based on Competitive Coding Scheme using Multi-scale Local Binary Pattern with Ant Colony Optimization

Yassir Aberni, Larbi Boubchir**, Boubaker Daachi

LIASD research Lab. – University of Paris 8
2 rue de la Liberté, 93526 Saint-Denis cedex, France

ABSTRACT

Among the various biometric traits that can be extracted from the hand, the palm vein structure that represents a reliable and secure source for identifying and/or verifying the identity of a person. Several recognition methods were proposed in the literature exploiting this modality; among them, the attractive approaches based on a competitive coding. Aiming to further improve the performance of these approaches, this paper presents a novel palm vein recognition method for personal authentication and identification based on a competitive coding scheme using Multi-scale local binary pattern (MLBP) with Ant colony optimization (ACO). ACO allows to override potential blocking points related to image quality or contrast problems that can be encountered with images from the Near infrared spectral band. The pre-processed images will be then sorted with a competitive coding scheme using MLBP; where the final image will be composed of the winning code from the different MLBP images. The matching process for making-decision is then performed using Kullback-Leibler divergence and Jaccard distance. The experimental results obtained on MS-PolyU database has shown that the proposed method achieves improved performances for both identification and verification modes up to 99.64% in terms of CIR for the identification and 0.00078% in terms of EER for the verification; and also outperforms the state-of-the-art methods.

1. Introduction

To be able to identify in a reliable way an individual within a group or a society, was always a necessity in order to protect oneself against fraud or theft, and new threats such as terrorism or cybercrime. To meet this need, several methods have emerged, but in the face of the logical evolution of international regulations, several so-called traditional methods have been replaced by new technological solutions.

The main purpose of identity management systems is to be able to establish an association between an individual and his/her identity when necessary. In addition, traditional mechanisms such as passwords and tokens do not provide solid evidence for the recognition of people. As a result, it is becoming more and more apparent that knowledge-based mechanisms and tokens alone are not enough to produce reliable identity management [1, 2].

Among the technologies also proposed for personal authentication and identification, biometrics quickly became the most relevant. It is considered as one of the main reliable sources for human recognition that has matured over time and has conquered many areas of our daily lives. A human biological characteristic of type physiological or behavioral, can be considered as a biometric characteristic if it meets the following conditions: (i) Universality: each person should have the characteristic, (ii) Distinctive: two people must be sufficiently different in terms of characteristic. (iii) Permanence: the characteristic must be sufficient invariant over a period of time, (iv) Collectability: the characteristic can be measured quantitatively [3].

Among the different modalities that exist, biometric recognition based on the palm vein can be considered among the most effective techniques in terms of accuracy and performance that delivers. In fact, the palm vein differs from the other biometric modalities by its intrinsic nature where the vein structure is not visible to the naked eye which reduces the possibility of stealing. Access to this biometric modality requires sophisticated hardware such as multispectral sensors that enable the acquisition of near-infrared images. The palm vein recognition can also represent some points of complexity, such as low contrast or image quality and the visibility of the venous structure that complicated the recognition phase. Faced with

**Corresponding author.
e-mail: larbi.boubchir@ai.univ-paris8.fr (Larbi Boubchir)

these problems, the efficiency of feature extraction method is paramount. Several palm vein methods have been proposed in literature [4] that can be regrouped into five main categories : (i) Structural-based approaches which are based mainly on the geometry of the vein, such as the minutiae, the curvatures and the lines [5, 6], (ii) Appearances-based approaches are methods that do not require a deep knowledge of the palm vein; and are often associated with meta-data analysis methods, such as Linear discriminant analysis (LDA), Independent component analysis (ICA) and Principal component analysis (PCA) [7, 8], (iii) Statistical approaches are divided into two sub-methods: a local representation which consists of dividing the palm vein image into several regions, a global representation where the whole palm vein image is taken into consideration [9, 10, 34], (iv) Coding-based approaches encode the multi-scale representation of palm vein images using a binary coding; where this kind of techniques is often implemented using Wavelet and Gabor filters [11, 12, 13, 14, 15, 30], and (v) Hybrid approaches consist of the combination of two or more techniques from the previous approaches that allow the benefits of each method to be tested, but it can be at the expense of time and performance [16, 33]. The vein structure can also be extracted from the dorsal side of the hand [36, 35], however, in this study we will focus only on the palmar venous structure.

In this paper, we propose a novel palm vein recognition method for personal authentication and identification. The proposed method is based on a competitive coding scheme using Multi-scale local binary pattern (MLBP) with Ant colony optimization (ACO). ACO has been implemented in order to be able to override potential blocking points related to image quality or contrast problems that can be encountered with images from the Near infrared spectral band (NIR[1]). Then the pre-processed images will be sorted with a competitive coding scheme using MLBP; where the final image will be composed of the winning code from the different MLBP images. The matching process for making-decision is then performed using Kullback-Leibler divergence and Jaccard distance.The experimental results obtained using MS-PolyU database have shown that the proposed method allows to achieve interesting performance in terms of the Correct identification rate (CIR) up ti 99.64% and up to 0.00078% in terms of Equal error rate (EER); and also outperforms some state-of-the-art methods.

The rest of the paper is organized as follows: Section 2 presents the related work. Section 3 describes our proposed palm vein recognition method while Section 4 illustrates the results of our experiments. Finally, Section 5 concludes the paper and presents some directions for future work.

2. Related work: a state-of-the-art overview

Various palm vein recognition methods have been proposed in the literature enriching the state-of-the-art. Among the methods identified, we have selected the most relevant ones that we have considered in our study.

For example, Lee et al. in [8] proposed an appearance method based on an analogous model, called modified 2D^{2}LDA. The classical LDA forms a vectorial space characterized by a smaller dimension to maximize the distance between classes and intra-classes, and has a limitation regarding its objective function which requires the non-singularity of one of the scatter matrices. This limitation can be restrictive in the case of palm vein recognition because the diffusion matrices are singular given that the data come from a very large space, which explains the number of data points is exceeded. The main difference between LDA and 2D^{2}LDA is that at the level of the data representation, 2D^{2}LDA uses a matrix representation as well as LDA uses a vectorized representation. The 2D^{2}LDA involves the eigendecomposition of matrices which are much smaller than the matrices in classical LDA. This reduces the time and space complexities [17]. Xin et al. [14] proposed a coding method based on the fusion of local Gabor histograms. The idea of their approach is to be able to decrease the sensitivity of the Gabor filter responses which can be related to the variations of luminous intensity and also to the change of positions the different samples of a given person. And, to further refine the results and increase the quality of the discriminant data from the filter response, a merge step to generate a uniform vector of local Gabor principal differences patterns (LGPDP) encoded data and the Local Gabor exclusive OR patterns (LGXP) was introduced. The LGPDP represents the palm vein feature derived from the Gabor magnitude response where each pixel of this response has a neighboring number of pixels. First, the pixels are quantized in different regions, then the Local maximum difference (LMD) is applied. This operator is to compare a central pixel with its environment and returns the maximum difference direction in the form of a binary sequence. The LGXP has been implemented to encode the Gabor phase response (GPR). Similar to the LGPDP operator, the LGXP is obtained by calculating the central pixel and its surrounding pixels. The same authors proposed in [13] a novel palm vein recognition scheme based on a coding method. The idea of their approach is to divide the normalized palm vein image into several non-overlapping sub-regions and then the optimal parameters of the Gabor filter will be determined from each sub-region. Thereafter, the extracted palm vein features will be encoded into vein code format. For the matching step, the minimum normalized Hamming distance algorithm was applied, which returns the minimum distance after multiple template displacements. This distance's value was used as the final score for template matching. Zhou et al. proposed in [12] a Neighborhood matching radon transform approach (NMRT). The purpose of this method is to accommodate the potential image deformations, translational, and rotational variations by matching to the neighborhood of the corresponding regions and generating more reliable matching scores. In [11], the author proposed a palm vein identification system for real-time personal identification by applying a low-cost NIR CCD camera-based palm vein device to capture the palm vein images. To represent a low-resolution palm vein image and match different palm vein images, an extended version of 2D Gabor filter is used to represent a palm vein image using its texture feature

[1]The near infrared (NIR) spectrum constitutes the electromagnetic waves in the region of 750 nm to 2000 nm wavelength.

with a normalized Hamming distance as a matching measurement. Bharathi et al. in [15] proposed a multimodal biometric system using vascular patterns of the hand such as finger vein and palm vein images. The features from these patterns are extracted using 2D Gabor filters with techniques based on gradient. The extracted features are then matched using the Euclidean distance metric, and are fused at the score level using fuzzy logic. In [5] Yan et al. proposed a structural method based on multi-sampling and feature-level fusion. This method implements the Scale-invariant feature transform (SIFT) to extract local characteristics from the different samples, and then reduces the redundant elements of these samples. This sorting will be based on comparing the angles between their feature vectors. Finally, the remaining features will be merged to generate the final model. The SIFT can be summarized in four main steps [5]: (i) adopt the difference of Gaussian to detect the extremes in the scale space, (ii) select the stable feature points from those extremes, (iii) assign a direction for each feature point, and (iv) generate the local feature descriptor. Ladoux et al. in [18] proposed an original method based on the use of Scale-invariant feature transform (SIFT) descriptors for the enrollment and the verification steps. The particularity of this method is that only one image is needed for the enrollment. Mirmohamadsadeghi et al. proposed in [19, 20] statistical methods based on high-order Local derivative patterns (LDPs) and a variety of multi-scale Local binary patterns (LBP). LDP represents a high-level texture descriptor for extracting first order non-directional models. It also retrieves derived direction variation information that is considered second-order pattern information. The pattern code is generated from the derivative direction of each neighboring pixel relative to the derivative of the central point. In [9], Kang et al. proposed an approach based on Mutual foreground LBP (MF-LBP) for contactless palm vein identification. First, the normalized gradient-based Maximal principal curvature (MPC) algorithm and k-means method are utilized for texture extraction. Second, based on the results of texture extraction, an LBP matching strategy was adopted for similarity measurements between the Mutual foreground (MF) of grayscale images. The MF is composed only of the extracted texture and its neighborhood of a grayscale image, which include the vast majority of useful distinctive information for identification while eliminating interference by excluding the background. The maximal matched pixel ratio was used to find the best matching region. Fronitasari et al. in [21] proposed a vein extraction method based on modified LBP descriptor combining with Probabilistic neural network (PNN) for the matching. Lu et al. in [33] proposed a palm vein recognition method based on a multi-scale Gaussian filter and the LBP descriptor. The multi-scale Gaussian filter is used to enhance vein patterns before feature extraction. Then, local binary patterns are extracted from the enhanced palm vein images. The resulting characteristics of the palm veins are illustrated as a binary series, allowing the similarities to be calculated efficiently by a binary operation. In [30], the authors proposed a multi-spectral palmprint recognition approach based on novel competitive coding scheme with oriented multiscale 2D log-Gabor filters. For the matching phase, matching measures have been proposed based on Bit-wise Hamming and KL distances.

Table 1 lists some state-of-the-art methods for palm vein recognition as well as their results obtained for the identification and verification modes.

3. Palm vein recognition: proposed method

Biometric recognition is based on so-called *recognition system* that allows the processing of biometric traits and the decision-making. In the case of palm vein recognition, a typical biometric system is constituted of three primary phases: (i) preprocessing and extraction of Region of interest (ROI), (ii) features extraction, and (iii) matching and decision-making. The following next subsections describe in detail all the phases constituting our proposed palm vein recognition system for personal identification and verification.

3.1. Preprocessing and ROI extraction

The ROI represents the main area from which the biometric characteristics will be extracted. This technique allows to standardize the treatment area and reduce the size of the samples which can reduce the processing time. Figure 1 shows a ROI image under the NIR band with 128×128 size. This image is captured with a Charge coupled device (CCD) composed of a camera, an A/D converter, lens, and a multispectral light source. The A/D converter is used to connect the computer with the CCD. The multispectral light makes it possible to control the type of output images from which the images used in our study come. The main objective of going through a preprocessing phase is to be able to align different palm vein images (the whole image or over a smaller area like ROI) and representing characteristics in a more sophisticated and discriminating form for ease the phase of comparison and recognition. To do this, several techniques have been proposed in literature such the ACO that we have used it in the proposed method in view of what it brings in terms of the wealth of characteristics. The next section describes this method.

3.2. ROI preprocessing based on ant colony optimization

The ACO is a heuristic method inspired by the movement of ant colonies in their way of looking for food. It is a stochastic method used to find solutions for many computational problems [22]. The main purpose of edge detection is to be able to identify changes in the intensity of the image, the ACO will be applied to detect the edges represented in the form of a pheromone matrix depending on the movements of the ants.

The ACO is based on an *exploration and exploitation* technique, the exploration phase is a procedure where the ants find the attractive path in the research area. The exploitation is to be able to find the best possible solution by the other members of the colony to be able to identify the most optimal way. The ACO can be described as follows: (i) the ants move from their nest $\mathcal{A}$ to the food $\mathcal{B}$. This movement is characterized by a random nature, and once the ant has found the food, it will leave on its path traces of pheromone. The repetitive movement of the ants on the path will allow strengthening the traces of pheromones on the shorter path; (ii) the strengthening of the

Table 1. Overview of the state-of-the-art methods for palm vein recognition.

Method	Approach type	Feature extraction	Database	Best result
Zhou et al [12] (2011)	Coding	Neighborhood Matching Radon Transform (NMRT)	MS-PolyU	Verification: EER=0.004% Identification: CIR=99.38%
Lee [8] (2015)	Appearance	Modified 2D^{2}LDA	Own	Verification: EER=0.01% Identification: CIR=99.41%
Xin et al. [13] (2017)	Coding	Adaptive 2D Gabor filter	CASIA	Verification: EER=0.38%
Kang et al. [9] (2014)	Statistical	MF-LBP	CASIA	Verification: EER=2.53%
Xin et al. [14] (2017)	Coding	LGPDP	CASIA	Verification: EER=0.18%
Lee [11] (2012)	Coding	Extended version of 2D Gabor filter	Own	Verification: EER=0.44% Identification: CIR=99.18%
Ladoux et al. [18] (2009)	Structural	SIFT	Own	Verification: EER=0.14%
Yan et al. [5] (2014)	Structural	SIFT + Feature-level fusion	CASIA	Verification: EER=0.16%
Mirmohamadsadeghi et al. [19] (2011) Mirmohamadsadeghi et al. [20] (2014)	Statistical	LBP + LDP	CASIA	Verification: EER=0.0009% Identification: CIR=97%
Fronitasari et al. [21] (2017)	Statistical	Modified LBP + PNN	CASIA	Identification: CIR=98%
Bharathi et al. [15] (2018)	Coding	2D Gabor filter + Gradient-based techniques	PUT Vein	Verification: EER=0.16% Identification: ACC=99.5%
Lu et al. [33] (2016)	Hybrid	Multi-scale Gaussian + LBP	MS-PolyU	Verification: EER=0.0017%
M. D. Bounneche et al. (2016) [30]	Coding	log-Gabor filter + Competitive coding + Hamming distance + KL Divergence	MS-PolyU	Verification: EER = 0.0274% Identification: IR rank-1=99.33%

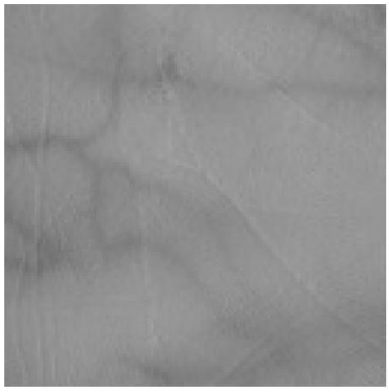

Fig. 1. An example of ROI from an palm vein image under NIR spectral band (image taken from MS-PolyU database [32]). ***The veins is clearly visible in NIR image.***

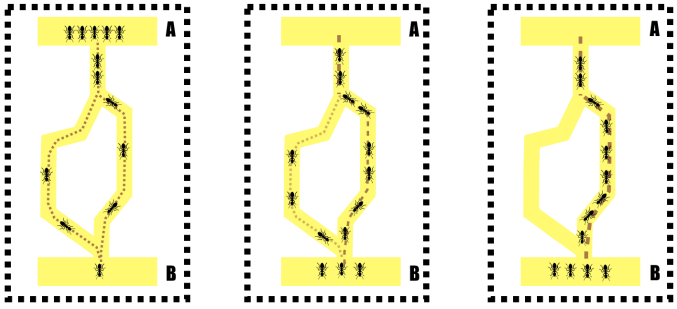

Fig. 2. Illustration of the principle of the ant colony.

pheromone on one of the routes taken by the ants will attract the entire colony to use the same path because on the longest paths the pheromone will evaporate over time. This principle is illustrated graphically by Figure 2

Several work have been carried out in relation to ACO, these works are classified according to 3 categories: (i) max-min, (ii) Ant system (AS), (iii) Ant colony system (ACS). To meet the need related to edge detection, techniques based on ACS [23] and techniques based on the AS [24] are the most used. The difference between the ACS and AS is that in the latter the pheromone values are updated only if the ant completed the tour. While the ACS uses a proportional pseudo-random rule to be able to exploit all the space of research, the evaporation of the pheromone is done in the case where the point of arrest belonging to the best so far tour. Every time an ant moves from a node to the other, it removes a certain amount of pheromone on this side to increase the exploration of the other edges (local pheromone update).

In the case of a 2D image, a set k of ants are applied to an image of size $M_1 \times M_2$, each pixel is considered as a node that serves as food for the ants. The goal is to find the optimal solution in the X search space to construct a pheromone matrix of entries representing the edge information.

The ACO algorithm consists of three main steps: (i) initialization process, (ii) iterative construction and update process, (iii) decision process.

(i) Initialization process:

During this phase, all the ants will be distributed in a random manner on the pixels of the image. The initial value of the pheromone on each element of the matrix is equal to a small non-null constant. The heuristic information matrix is constructed based on the local variation of the intensity values; and it is determined during initialization since it is dependent only on the pixel values of the image, thus, constant [23].

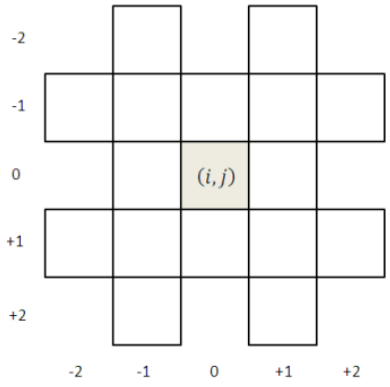

Fig. 3. A local configuration for computing the intensity variation at the pixel (i, j)**.**

For a given pixel (i, j), the heuristic information is determined by the local statistics:

$$\eta_{i,j} = \frac{V_c(I_{i,j})}{V_{max}} \tag{1}$$

where $I_{i,j}$ is the intensity value of the pixel at (i, j). $V_c(I_{i,j})$ is a function that acts on the local group of pixels around the pixel (i, j) and it given by (see Figure 3):

$$\begin{aligned} V_c(I_{i,j}) = &\left|I_{i-2,j-1} - I_{i+2,j+1}\right| + \left|I_{i-2,j+1} - I_{i+2,j-1}\right| \\ &+ \left|I_{i-1,j-2} - I_{i+1,j+2}\right| + \left|I_{i-1,j+2} - I_{i+1,j-2}\right| \\ &+ \left|I_{i-1,j-1} - I_{i+1,j+1}\right| + \left|I_{i-1,j+1} - I_{i+1,j-1}\right| \\ &+ \left|I_{i-1,j} - I_{i+1,j}\right| + \left|I_{i,j-1} - I_{i,j+1}\right| \end{aligned}$$

$V_{\max}$ is the maximum intensity variation in the whole image and serves as a normalization factor. It is defined as fellows:

$$V_{\max} = \sum_{M_1}^{i=1} \sum_{M_2}^{j=1} V_c(I_{i,j}) \tag{2}$$

(ii) Iterative construction and update process

At the construction stage, an ant is randomly selected to move on the image for the movement step until it has made L construction steps. An ant moves from (i_0, j_0) the pixel to an adjacent pixel (i, j) depending on the pseudorandom proportional rule. The probability of movement between the two pixels is given by:

$$P^{(n)}_{(i_0,j_0)(i,j)} = \frac{(\tau^{(n-1)}_{i,j})^{\alpha}(\eta_{i,j})^{\beta}}{\sum_{(i,j)\in\Omega_{(i_0,j_0)}}(\tau^{(n-1)}_{i,j})^{\alpha}(\eta_{i,j})^{\beta}} \tag{3}$$

where $\tau^{(n-1)}_{i,j}$ is the pheromone value for pixel (i, j) and $\Omega_{(i_0,j_0)}$ is the neighborhood pixels of pixel (i_0, j_0). $(\eta_{i,j})$ represents the value of heuristic matrix at the node (i, j). The value of the constants α and β control the influences the pheromone matrix and heuristic matrix, respectively.

The first update is done on the pheromone matrix after each ant is moved within each n^{th} construction step, the amount of pheromone on the pixel is updated based on the equation for ACS local pheromone update :

$$\tau^{(n)}_{i,j} = (1 - \varphi).\tau^{(n)}_{(i,j)} + \varphi.\tau_{init} \tag{4}$$

where $\varphi \in [0, 1]$ is the pheromone decay coefficient and τ_{init} is the initial pheromone value.

After all the ants finish the construction process, global pheromone update is performed on pixels that have been visited by at least one ant:

$$\tau^{(n)}_{i,j} = (1 - \rho).\tau^{(n-1)}_{i,j} + \rho.\sum_{K=1}^{K} \Delta\tau^{(k)}_{i,j} \tag{5}$$

where $\tau^{(k)}_{i,j}$ is the amount of pheromone deposited by the k_{th}.

(iii) Decision process

In the decision phase, a technique called Otsu thresholding [25] has been implemented to determine the threshold from which the pixel resulting from the final pheromones matrix can be considered as edge or non-edge.

An example of the final image after using the ACS is illustrated in Figure 4. The parameters used are $k = 256$ (128×128 ROI image) and $\tau_{init} = 0.1$

Fig. 4. ACO-based edge detection. ***An example of edge detection using ACS applied on the ROI image illustrated in Figure 1.***

3.3. Multi-scale local binary pattern

Among the various image texture descriptors, LBP has proven its effectiveness in extracting the palm features in a general way and particularly the palm vein. The LBP operator was proposed to describe the texture from the contrast differences [26]. It's a texture descriptor, which is based on the grey-level comparison of a neighbourhood of pixels [20, 33]. For the central pixel, the neighborhood $R \times R$ of P pixels is compared with the value of the central pixel, and the result is considered as the decimal equivalent of a binary number. For a given image I, LBP descriptor is computed for each pixel c using the following equation:

$$LBP_{P,R}(I_c) = \sum_{p=1}^{P} s(Z_p - Z_c)2^{p-1} \tag{6}$$

where P and R are respectively the radius of the neighbourhood and the number of neighbouring pixels. $s(u) = 1$ if $u \geq 0$ and 0 otherwise. Z_p is one of the P neighbours of Z_c. Figure 5 shows an example of LBP neighbourhoud with $P = 16$ and $R = 7$.

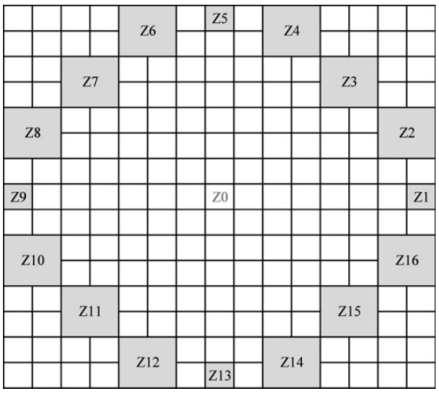

Fig. 5. An example of LBP neighbourhoud. Z_0 ***is the reference pixel and*** $\{Z_1, Z_2, \ldots, Z_{16}\}$ ***represent its neighbours with*** $P = 16$ ***and*** $R = 7$.

Indeed, the palm vein is characterized by a linear form, a variable width and a level of gray different from the background. Given that the LBP can extract these characteristics according to the level of gray then, the integration with the palm vein makes it possible to extract the most discriminating parts. The LBP has been modified to be compatible with the special pattern, more specifically the LBP uniform which allows to extract the schemas with a maximum of two binary transitions [27]. The vein either crosses the local neighbourhood or ends inside; this means that there will not be many discriminating binary transitions relative to the change of gray level. Which explains the choice of the uniform pattern since we will have at most two binary transitions in their binary form. As explained in section 3.2, the ACO was applied to reduce the dimensionality by feature selection. Instead of using original image, the MLBP will be directly applied to the extracted image with the ACO. This will optimize the processing fields and have more discriminating biometric features. Figure 6 shows an example of LBP image generated from the palm vein image shown in Figure 1.

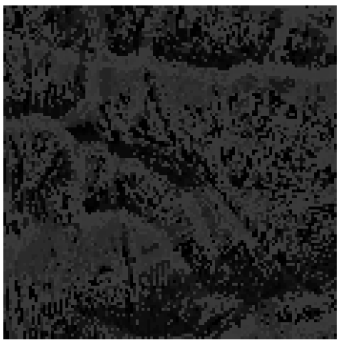

Fig. 6. LBP image generated from the ROI image of the palm vein shown in Figure 1.

3.4. MLBP-based competitive coding

The principle of MLBP is to apply a multi-scale representation based on LBP where the goal is to extract several LBPs with different radius of the neighbourhood R with different number of neighbouring for the pixels considered P [20]. In this work, we have defined a competitive coding scheme based on Gabor filters and combined with MLBP. Basically, the proposed competitive coding scheme employed multiple 2D Gabor filters to extract the orientation information from palm lines. It uses a competitive rule *winner-takes-all* using the palm line contrast.

The proposed feature extraction scheme is based on the competitive radius coding where the dominant radius of the multi-resolution LBP (radius and neighbourhood) are encoded. The winner scale and orientation indexes for each element from the filtered images, denoted $\binom{R}{P}$, can be computed as :

$$\binom{R}{P} = \max\left(LBP_{(R,P)}(x, y)\right) \tag{7}$$

where $LBP_{(R,P)}$ is the LBP descriptor at radius R and P neighbourhood. (x, y) represents the spatial location of each element.

To encode the winning element, we used a technique based on the Gray code that consists of replacing the element resulting from Eq. 7 with its value *gray code*. The Gray code is used to make a correspondence of the value (radius-neighbourhood) with a binary value (only five binary codes have been considered in the experiments corresponding to five radius values for R). In general, the Gray code is used to avoid transient states and also facilitate the correction of errors in digital communication.

Table 2 illustrates different bitwise representations to encode five states corresponding to five different radius for MLBP. Only 3 bits are necessary to encode these states using Gray code. Figure 7 shows an example of LBP images generated for different radius (i.e. $R = \{1, 2, \ldots, 5\}$) with $P = 8$.

Figure 8 shows the feature map generated from the ACO image shown in Figure 4 using the proposed competitive coding scheme based on MLBP and Gray binary coding.

Table 2. Bit representation of the multi-scale coding based on Gray binary code. ***An example to encode five states corresponding to five different radius for MLBP with*** $P = 8$***. Only 3 bits are necessary to encode these states using Gray code.***

Neighbourhood P	Radius R	Bit 0	Bit 1	Bit 2
8	1	0	0	0
	2	0	0	1
	3	0	1	1
	4	0	1	0
	5	1	1	0

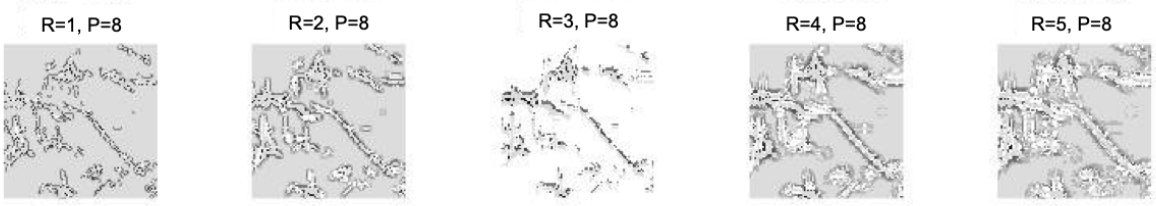

Fig. 7. An example of LBP images along five radius (with $P = 8$**) generated from the ACO image shown in Figure 4.**

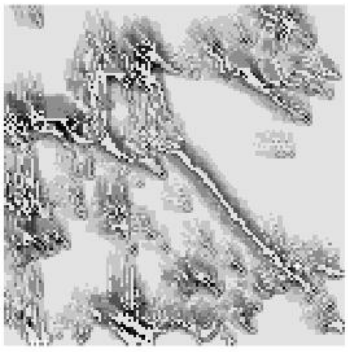

Fig. 8. An example of the feature map generated from the ACO image shown in Figure 4 using our proposed competitive coding scheme based on MLBP and Gray binary coding.

3.5. Matching process

The matching and decision step consists in checking the level of similarity between the feature maps. Based on the similarity score computed, a decision is made concerning the identification or the verification of a user (e.g. accepting or rejecting the requested user).

Two measures of similarity were proposed in our work; where the first one is based on the Kullback–Leibler (KL) divergence, and the second is based on the distance of Jaccard. Both measures proposed are compatible with bitwise form data.

3.5.1. Kullback–Leibler divergence

The KL divergence is a measure of dissimilarity between two probability distributions [28, 29]. It is defined as fellow:

$$d_{KL}(P,Q) = \sum_{j=0}^{(M-1)(N-1)} \sum_{i=1}^{B} P_i(j) \log\left(\frac{P_i(j)}{Q_i(j)}\right) \tag{8}$$

$P_i(j)$ and $Q_i(j)$ are the vectors of size $(1 \times MN)$ of the stored and tested palm vein feature maps P and Q, respectively. B is the number of bits used for Gray code. As is shown in (an example of feature map is illustrated in Figure 8).

In this study, a normalization of D_{KL} is performed to allow a comparison of two distances as follows [30]:

$$D_{KL}(P,Q) = \frac{d_{KL}(P,Q) - \min\left(d_{KL}(P,Q)\right)}{\max\left(d_{KL}(P,Q)\right) - \min\left(d_{KL}(P,Q)\right)} \tag{9}$$

where D_{KL} is the normalized distance. $\min\left(d_{KL}(P,Q)\right)$ and $\max\left(d_{KL}(P,Q)\right)$ are respectively the minimum and maximum of the non-normalized d_{KL}.

3.5.2. Jaccard distance

The Jaccard distance is defined as *Intersection* over *Union*. It can be represented as:

$$J(P,Q) = \frac{|P \bigcap Q|}{|P \bigcup Q|} = \frac{|P \bigcap Q|}{|P| + |Q| - |P \bigcap Q|} \tag{10}$$

Or A and B are two sets of the same size and nature. Jaccard's distance proved to be compatible with sets of binary values. Let two sets P and Q, in each of them, there exists a set of binary attributes, with a value of 0 or 1 [31]:
$P = (a_1, a_2, a_3, ..., a_n)$
$Q = (b_1, b_2, b_3, ..., b_n)$
Since P and Q, we can deduce quantities according to binary classification:
S_{11}: number of attributes that are worth 1 in P and Q
S_{01}: number of attributes that are 0 in P and 1 in Q
S_{10}: number of attributes that are 1 in P and 0 in Q
S_{00}: number of attributes that are 0 in P and Q
This means that each pair of compared values of P and Q will necessarily belong to one of the four categories. The Jaccard index becomes :

$$J = \frac{S_{11}}{S_{01} + S_{10} + S_{11}} = \frac{S_{11}}{n - S_{00}} \tag{11}$$

In our case, a normalized form was used to calculate the distance of Jaccard :

$$D_J = 1 - \frac{\sum_{j=0}^{MN-1} \sum_{i=1}^{B} P_i(j) \otimes Q_i(j)}{\sum_{0}^{MN-1} \sum_{i=1}^{3} P_i(j) \oplus Q_i(j)} \tag{12}$$

where P and Q represent respectively the stored and tested multi-resolution palm vein feature maps. P_i and Q_i are their i^{th} bit. N and M are the size of the palm vein image while (x, y) indicates the element's location. B is the number of bits used for Gray code.

The general diagram of our proposed method is illustrated in Figure 9.

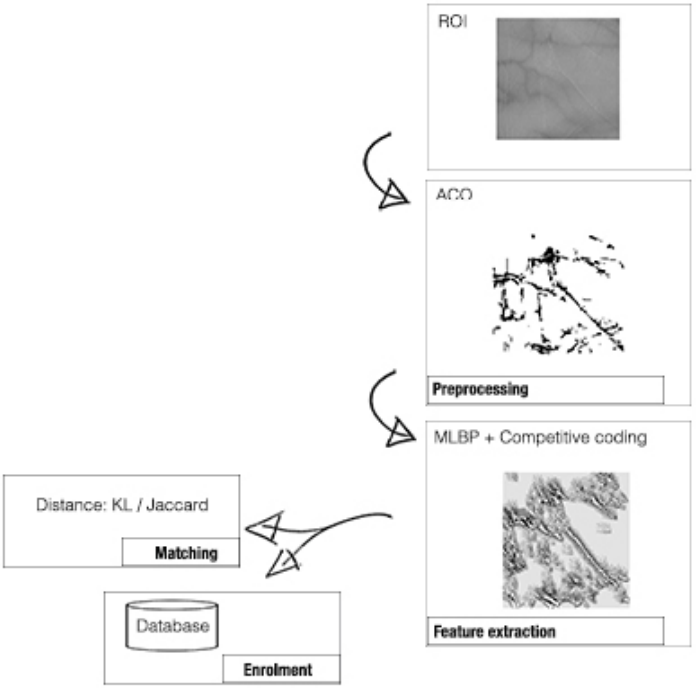

Fig. 9. Palm vein recognition process flow diagram.

4. Experiments and results

To evaluate our methods as well as the results obtained, we have used the MS-PolyU database described in the next subsection 4.1. The results obtained for the verification and identification modes are firstly computed from samples of different LBP descriptors (i.e. LBP images in Figure 7). Then, the results obtained from the proposed method are analyzed and compared with some existing methods of the state-of-the-art.

4.1. Database

MS-PolyU is among the popular multispectral palm-print database. It contains 6000 images from 250 volunteers, including 195 males and 55 females, with an age ranging between 20 and 60 years [32]. In our study, we have exploited only the images from the NIR spectral band to exploit the palm vein structures. Indeed, the NIR band can cross the muscle tissues and detect the venous structure.

4.2. MLBP descriptor

The purpose of this test is to assess the performance of the parameters of the LBP descriptor. The variation of the different radius values made it possible to have different CIR values according to the distance used. The results obtained demonstrate the compatibility of the radius R and neighborhood P values used with the size of the ROI image and the biometric characteristics included in it. For example, in Tables 3 and 4, the maximum value corresponds to the uniform $LBP_{(8,4)}$ (i.e. $P = 8$ and $R = 4$). This result is consistent with the width size of the veins in the image which varies between 2 and 8 pixels. An exemple is illustrated in Figure 10.

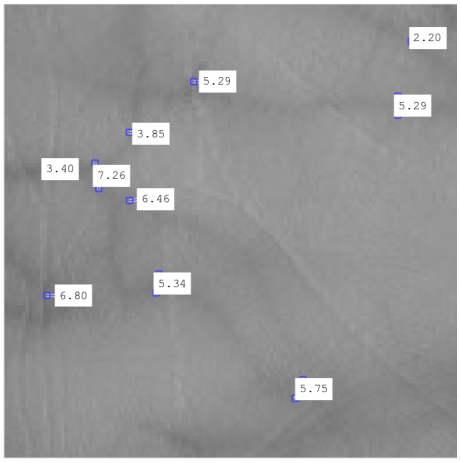

Fig. 10. An example of a palm vein image with the width veins size in pixels. ***An example of ROI image with size*** 128×128.

4.3. Identification and verification

We have assessed the performance of our proposed method for the both verification and identification modes: (i) verification mode which consists in comparing the identity claimed by the person and his biometric data, (ii) identification mode which consists in comparing the biometric characteristics of entries

Table 3. Identification results (in terms of CIR) of the proposed methods based on LBP operators with uniform mapping for different radius values with a number of neighbourhood equal to 8. ***D_{KL} and D_J represent respectively the KL and Jaccard distances.***

Distance	Radius				
	1	2	3	4	5
D_{KL}	86.80%	87.23%	88%	**90%**	87.34%
D_J	86%	88.67%	90.30%	**91.45%**	88.35%

Table 4. Verification results (in terms of EER) of the proposed methods based on LBP operators with uniform mapping for different radius values with a number of neighbourhood equal to 8. ***D_{KL} and D_J represent respectively the KL and Jaccard distances.***

Distance	Radius				
	1	2	3	4	5
D_{KL}	0.009%	0.0084%	0.008%	**0.0065%**	0.0075%
D_J	0.0087%	0.0083%	0.0076%	**0.0069%**	0.008%

with those stored in database. MS-PolyU offers two set images collected in two separate sessions. each set contains a selection of six images of each hand. To organize the database, we have considered that one of the collections represents the test and the second is the gallery. Each feature map from the test set was matched with all the maps in the gallery set using both distances defined in Eqs. 9 and 12.

The following metrics: EER and CIR, are used to assess the recognition performances for the verification and identification modes. Noted that during the matching phase, we took into consideration the translation's effect that can occur at the time of the ROI extraction. Indeed, for each test map we apply horizontal and vertical translations before calculating the distance with the same template. The test map was moved from -5 to 5 vertically and horizontally, and a distance is calculated between the same model and those obtained by each translation where the minimum value is chosen as the best and most similar.

Identification results

As discussed in Section 2, we have studied the existing methods for palm vein recognition in order to identify the most relevant of them by studying their feature extraction, matching process, and recognition performances. Table 5 illustrates the best results obtained for the identification mode in terms of CIR. By analyzing the results shown, we can notice that our proposed methods outperform the state-of-the-art methods such as the methods in [12] and [30]. Indeed, the proposed methods allow to achieve a higher CIR up to 99.64%.

The overall identification performances of the proposed methods with KL and Jaccard distances were assessed using the Cumulative match curve (CMC). The CMC curve results are shown in Figure 11. By analysing the results obtained, we notice that the use of Jaccard distance allows improving the recognition performance than the use of KL distance.

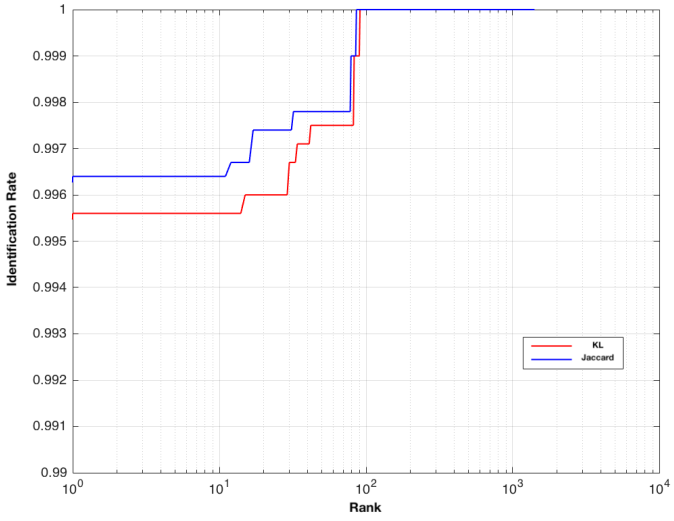

Fig. 11. CMC curves of the proposed methods using KL and Jaccard distances.

Verification results

We have evaluated the performances of the proposed methods for the verification mode and compared them with the performances of some state-of-the-art methods such as the methods in [33, 34, 12]. Table 6 illustrates the results obtained in terms of EER. By analyzing these results, we can notice that the proposed method with KL distance achieves a lowest EER (up to 0.00078%) compared to the rest of the existing methods; and also outperforms the proposed method with Jaccard distance. Furthermore, the computation of MLBP descriptor on the ACO images allows to achieve best results compared to the methods using the LBP descriptors such as the method in [33]. In addition, MLBP was able to extract more precise biometric characteristics depending on the width of the features, and the action of combining all this information and putting it in a single image, this will allow to have a final image that groups together most discriminating data of each descriptor.

The overall verification performances of the proposed methods with KL and Jaccard distances were assessed using the Receiver operating characteristic curve (ROC). The ROC curve results are shown in Figure 12. By analyzing the results obtained, we notice that the use of Jaccard distance allows improving the recognition performance than the use of KL distance.

Table 5. Comparing the identification results of the proposed methods with the state-of-the- art methods.

Methods	Feature extraction	Distance for matching	Database	CIR
M. D. Bounneche et al. [30] (2016)	log-Gabor filter + Competitive coding	Bitwise Hamming	MS-PolyU	99.33%
Zhou et al. [12] (2011)	NMRT	Bitwise Hamming	MS-PolyU	99.38%
Proposed method 1	ACO + MLBP + Competitive coding	KL	MS-PolyU	99.56%
Proposed method 2	ACO + MLBP + Competitive coding	Jaccard	MS-PolyU	99.64%

Table 6. Comparing the verification results of the proposed methods with the state-of-the-art methods.

Methods	Feature extraction	Distance	Database	EER
Lu et al. [33] (2016)	Multi-scale Gaussian + LBP	Binary operation	MS-PolyU	0.0017%
Wang et al. [34] (2018)	Deep neural network (DNN)		MS-PolyU	0.068%
Zhou et al. [12] (2011)	NMRT	Bitwise Hamming	MS-PolyU	0.004%
Proposed method 1	ACO + MLBP + Competitive coding	KL	MS-PolyU	0.00078%
Proposed method 2	ACO + MLBP + Competitive coding	Jaccard	MS-PolyU	0.0015%

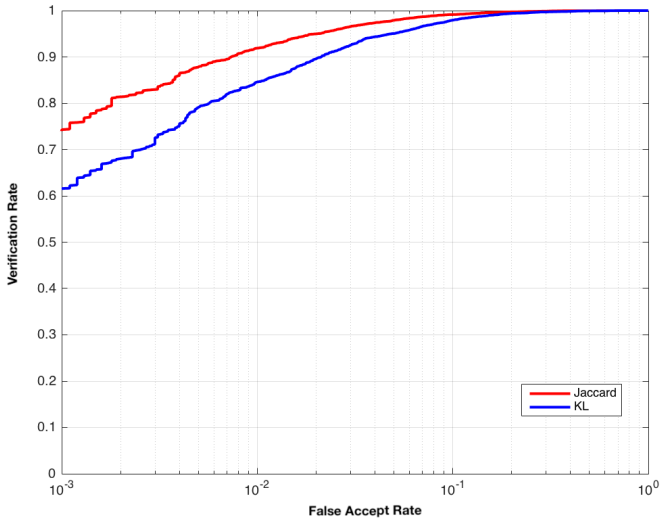

Fig. 12. ROC curves of the proposed methods using KL and Jaccard distances.

Table 7. Execution time of the proposed method. ***The execution time (average time over 20 runs) for feature matching step is given for the both distances.***

Step	Execution time (s)
Preprocessing with ACO	0.126
Feature extraction (MLBP + Competitive coding)	0.215
Feature matching	
(1) KL distance	0.0016
(2) Jaccard distance	0.0023

4.4. Speed performance

The proposed method was implemented using Matlab R2015b on a MacBook Pro with OS X High Sierra, Intel Core i7 CPU (2.5 GHz) and 16 GB RAM. Table 7 shows the results obtained in terms of execution time (average time over 20 runs). We can see that the preprocessing and feature extraction phases take more time compared to the matching phase but it remains below than 1s. The total processing time using the KL distance is about 0.34s and 0.35s for Jaccard distance which are much similar. With these processing times, the proposed method can be used within the framework of real-time application.

5. Conclusion

A novel approach for palm vein recognition was proposed in this paper. The proposed method is based on a competitive coding scheme using MLBP; where the ACO was applied on the palm vein images in order to enhance the quality of their feature maps generated from MLBP. Two distance metrics based on KL and Jaccard have been proposed for the matching. The experimental results on MS-PolyU database have shown that the proposed method achieves improved performances for both identification and verification modes up to 99.64% in terms of CIR for the identification and 0.00078% in terms of EER for the verification. Furthermore, the proposed method outperforms the state-of-the-art methods considered in our study. Our future work will be focused on the improvement of the proposed approach by analyzing other multi-scales representations able to capture discriminative information from palm vein images and thus enhance the recognition performance. Other distances for the matching can be also investigated.

References

[1] A. K. Jain, A. Ross and K. Nandakumar, *Introduction to Biometrics*, Springer Ed., 2011.
[2] S. Z. Li, and A. Jain, *Encyclopedia of Biometrics*, Springer Ed., 2015.
[3] A. K. Jain, A. Ross and S. Prabhakar, *An Introduction to Biometric Recognition*, IEEE Transactions on Circuits and Systems for Video Technology, vol. 14, no. 1, pp. 4–20, 2004.
[4] Y. Aberni, L. Boubchir and B. Daachi, *Multispectral Palmprint Recognition: A Survey and Comparative Study*, Journal of Circuits, Systems and Computers, vol. 28, no. 7, pp. 1–25, 2019.
[5] X. Yan, W. Kang, Q. Wu and F. Deng, *Palm vein recognition based on multi-sampling and feature-level fusion*, Neurocomputing, vol. 151, no. 2, pp. 798–807, 2015.

[6] Y. Zhou, Y. Liu , Q. Feng , F. Yang, J. Huang and Y. Nie, *Palm-Vein Classification Based on Principal Orientation Features*, PLOS ONE , vol. 9, no. 11, e116446, 2014.

[7] S. Elnasir and S. M. Shamsuddin, *Proposed scheme for palm vein recognition based on Linear Discrimination Analysis and nearest neighbour classifier*, International Symposium on Biometrics and Security Technologies (ISBAST), 2014.

[8] Y. P. Lee, *Palm vein recognition based on a modified (2D)^{2}LDA*, Signal, Image and Video Processing, vol. 9, issue. 1, pp. 229–242, 2015.

[9] W. Kang and Q. Wu, *Contactless palm vein recognition using a mutual foreground-based local binary pattern*, IEEE Transactions on Information Forensics and Security, vol. 9, no. 11, pp. 1974–1985, 2014.

[10] E. Piciucco, E. Maiorana and P. Campisi, *Palm vein recognition using a high dynamic range approach*, IET Biometrics ,vol. 7, no. 5, pp. 439–446, 2018.

[11] J. C. Lee, *A novel biometric system based on palm vein image*, Pattern Recognition Letters, vol. 33, no. 12, pp. 1520–1528, 2012.

[12] Y. Zhou and Y. A. Kumar, *Human identification using palm-vein images*, IEEE Transactions on Information Forensics and Security, vol. 6, no. 4, pp. 1259–1274, 2011.

[13] M. Xin, J. Xiaojun, H. Hai, C. Yuanhao and M. Junsheng, *Palm vein recognition scheme based on an adaptive Gabor filter*, IET Biometrics, vol. 6, no. 5, pp. 325–333, 2017.

[14] M. Xin and J. Xiaojun, *Palm vein recognition method based on fusion of local Gabor histograms*, The Journal of China Universities of Posts and Telecommunications, vol. 24, no. 6, pp. 55–66, 2017.

[15] S. Bharathi and R. Sudhakar, *Biometric recognition using finger and palm vein images*, Soft Computing, vol. 23, no. 6, pp. 1843–1855, 2018.

[16] O. E. Olusayo, O. J. Babalola and I. W. Oladimeji, *Palm vein recognition system using hybrid principal component analysis and artificial neural network*, International Journal of Advanced Research in Computer Science and Software Engineering, vol. 3, no. 7, pp. 69–78, 2013.

[17] J. Ye, R. Janardan and Q. Li, *Two-Dimensional Linear Discriminant Analysis*, Advances in Neural Information Processing Systems (NIPS), 2004.

[18] P. O. Ladoux, C. Rosenberger and B. Dorizzi, *Palm vein verification system based on SIFT matching*, International Conference on Biometrics (ICB), pp. 1290–1298, 2009.

[19] L. Mirmohamadsadeghi and A.Drygajlo, *Palm Vein Recognition with Local Binary Patterns and Local Derivative Patterns*, International Joint Conference on Biometrics (IJCB), 2011.

[20] L. Mirmohamadsadeghi and A. Drygajlo, *Palm vein recognition with local texture patterns*, IET Biometrics, vol. 3, no. 4, pp. 198–206, 2014.

[21] D. Fronitasari and D. Gunawan, *Palm Vein Recognition by using modified of Local Binary Pattern (LBP) for Extraction Feature*, The 15th International Conference on Quality in Research (QiR): International Symposium on Electrical and Computer Engineering, 2017.

[22] M. Dorigo and L. M. Gambardella, *Ant colony system: a cooperative learning approach to the traveling salesman problem*, IEEE Transactions on Evolutionary Computation, vol. 1, no. 1, pp. 53–66, 1997.

[23] A. V. Baterina and C. Oppus,*Image Edge Detection using Ant Colony Optimization*, WSEAS Transactions on Signal Processing archive, vol. 6, no. 2, pp. 58–67, 2010.

[24] J. Tian, W. Yu and S. Xie, *An Ant Colony Optimization Algorithm for Image Edge Detection*, IEEE Congress on Evolutionary Computation (IEEE World Congress on Computational Intelligence), pp. 751–756, 2008.

[25] N. Otsu, *A Threshold Selection Method from Gray level Histograms*, IEEE Transactions on Systems, Man and Cybernetics, vol. 9, no. 1, pp. 62–66, 1979.

[26] M. Pietikainen, A. Hadid, G. Zhao and T. Ahonen, *Computer vision using local binary patterns*, Springer Ed., 2011.

[27] T. Ojala, M. Pietikainen, T. Maenpaa, *Multiresolution gray-scale and rotation invariant texture classification with local binary patterns*, IEEE Transactions on Pattern Analysis and Machine Intelligence, vol. 24, no. 7, pp. 971–987, 2002.

[28] S. Kullback and R. Leibler, *On information and sufficiency*, Annals of Mathematical Statistics, vol. 22, pp. 79–86,1951.

[29] A.C.S. Chung, W.M. Wells, A. Norbash and W.E.L. Grimson, *Multimodal image registration by minimising Kullback–Leibler distance*, International Conference on Medical Image Computing and Computer Assisted Intervention (MICCAI), The Series of Lecture Notes in Computer Science, vol. 2489, pp. 525–532, 2002.

[30] M. Bounneche, L. Boubchir, et al., *Multi-spectral palmprint recognition based on oriented multiscale log-Gabor filters*, Neurocomputing, vol. 205, pp. 274–286, 2016.

[31] P. Jaccard, *Distribution de la flore alpine dans le Bassin des Dranses et dans quelques regions voisines*, Bulletin de la Société Vaudoise des Sciences Naturelles, 37, 241–272, 1901.

[32] PolyU Multi-spectral Palmprint Database, `http://www4.comp.polyu.edu.hk/biometrics/MultispectralPalmprint/MSP.htm`

[33] W. Lu, M. Li and L. Zhang, *Palm Vein Recognition Using Directional Features Derived from Local Binary Patterns*, International Journal of Signal Processing, Image Processing and Pattern Recognition vol. 9(5), pp. 87–98, 2016.

[34] J. Wang, Z. Pan, G. Wang, et al., *Spatial Pyramid Pooling of Selective Convolutional Features for Vein Recognition*, IEEE Access, vol. 6, pp. 28563–28572, 2018.

[35] S. Joardar and A. Chatterjee, *Palm Dorsa Vein Pattern based biometric verification system using Anisotropic Generalized Procrustes Analysis on weighted training dictionary*, Applied Soft Computing, vol. 85, 105562, 2019.

[36] S. Joardar, A. Chatterjee, S. Bandyopadhyay, et al., *Multi-size patch based collaborative representation for Palm Dorsa Vein Pattern recognition by enhanced ensemble learning with modified interactive artificial bee colony algorithm*, Engineering Applications of Artificial Intelligence, vol. 60, pp. 151–163, 2017.